Quenching and excitation transfer in the $n=3$ helium sublevels in a low-pressure glow discharge

B. Dubreuil* and A. Catherinot

Groupe de Recherches sur l'Energétique des Milieux Ionisés, Université d'Orléans, 45045 Orleans Cedex, France

(Received 4 June 1979)

The collisional and radiative processes leading in a glow discharge to quenching and excitation transfer in the $n=3$ helium sublevels are investigated by means of a laser perturbation method. Laser-induced population perturbations are solutions of coupled rate equations, the coefficients of which are related to radiative coefficients and collisional excitation cross sections. An accurate numerical method of data analysis (the "identification method") is developed in which the rate coefficients are determined so as to minimize the difference between experimental curves and those calculated from the model. In the pressure and current intensity investigated, $P<10$ Torr, $i<50$ mA, only radiative and atom-atom collision processes contribute to quenching and excitation transfer in the $n=3$ levels. Numerical identification of the $n=3$ experiments provides a nearly complete set of rate coefficients and thermally averaged cross sections. In particular, $3\,^1P \rightleftarrows 3\,^1D$ excitation transfers predominate over the $3\,^3P \rightleftarrows 3\,^3D$ ones. This results from the near-resonant character of the He–He* inelastic collision processes.

I. INTRODUCTION

Excitation transfers between excited states play an important part in the formation of quasistationary atomic-state populations in non-local-thermodynamic-equilibrium (LTE) plasma such as low-pressure and low-current glow discharges.

Excitation transfers by inelastic atomic or molecular collisions are responsible for lasing in a great number of gas lasers, or on the contrary can be limiting factors to population-inversion processes as for the $3\,^1P$-$3\,^1D$ ($\lambda_L = 95.8\ \mu$m) laser transition observed in a helium glow discharge.[1]

In a low-pressure ($P_a < 10$ Torr), low-current ($i < 50$ mA) helium glow discharge, excitation of the ground-state atoms is ensured by electronic inelastic collisions. Then, under continuous electrical excitation, a quasistationary equilibrium sets up, in which excitation processes are on the whole balanced by radiative, collisional depopulating processes: emission and absorption of radiation, inelastic collisions with electrons and atoms, and diffusion towards the walls of the discharge tube.

The aim of this paper is to present an investigation of these quenching mechanisms for the $n=3$ helium sublevels in the positive column of a low-pressure, low-current glow discharge, and particularly atom-atom collisional excitation transfers of the type

$$\mathrm{He}(3^{2S+1}L) + \mathrm{He}(1\,^1S) \rightarrow \mathrm{He}(3\,^{2S+1}L') + \mathrm{He}(1\,^1S) + \Delta E \qquad (1)$$

which predominate in a weakly ionized gas.

These mechanisms have been studied in helium afterglows,[2] in helium glow discharges,[3] and in helium–electron-beam interactions[4,5] by conventional emission or absorption optical spectroscopy.

Interpretation of measurements obtained in these experiments are often complicated owing to the mixing of a great number of populating and depopulating processes which connect the particular studied level with the whole set of excited states.

An increase of selectivity, while keeping maximum information on a particular class of processes, can be obtained from time-resolved laser perturbation studies. These experimental methods were developed recently by several groups in the field of plasma physics[6–9] and in our laboratory. For instance, we have investigated some processes in helium,[10–12] argon,[13] and hydrogen[14,15] glow discharges.

While this method has been previously described, it seems to us important to recall its principles so as to point out the characteristics of the numerical procedure of data analysis we have elaborated. This numerical "identification method" leads to the determination of reaction rates from time-resolved measurements and can be used in connection with general physical or chemical-kinetic studies.

This procedure is applied to the $n=3$ helium-state perturbation experiments and provides quenching and excitation transfer cross sections with good accuracy.

II. POPULATION RATE EQUATIONS

In an atomic ionized gas, the population rate equations taking into account optical pumping can be generally written:

$$\frac{dN_i}{dt} = -N_i\left(\sum_{k<i}(A_{ik}\Lambda_{ik}) + n_a\sum_{k\neq i}R_{ik} + n_e\sum_{k\neq i}S_{ik}\right) + \sum_{j\neq i}N_j(A_{ji}\Lambda_{ji} + n_aR_{ji} + n_eS_{ji}) + n_e^2(n_a r_i + s_i)$$
$$+ \delta_{ia}N_b n_p\sigma_{ba}L(t) - \delta_{ib}N_b n_p\sigma_{ba}L(t), \quad N_i(t_0) = N_i^0, \quad i = 1,2,\ldots,b,\ldots,a,\ldots \tag{2}$$

where N_i represents the $|i\rangle$-state population, and other terms are defined below.

The following processes have been taken into account: spontaneous emission of radiation (Λ_{ij}, optical escape factor),

$$|i\rangle \xrightarrow{A_{ij}\Lambda_{ij}} |j\rangle + h\nu_{ij};$$

atom-atom collision excitation transfer,

$$|i\rangle + |\text{ground state}\rangle \xrightarrow{R_{ij}} |j\rangle + |\text{ground state}\rangle + \Delta E;$$

electron-atom inelastic collisions,

$$|i\rangle + e^- \xrightarrow{S_{ij}} |j\rangle + e^- + \Delta E;$$

three-body recombination,

$$|\text{ion}\rangle + e^- + |\text{ground state}\rangle \xrightarrow{r_i} |i\rangle + |\text{ground state}\rangle;$$

radiative recombination,

$$|\text{ion}\rangle + e^- \xrightarrow{s_i} |i\rangle + h\nu;$$

laser pumping,

$$|b\rangle + h\nu_L \xrightarrow{n_p\sigma_{ba}L(t)} |a\rangle,$$

where σ_{ba} represents the absorption rate at laser frequency, and n_p, $L(t)$ are, respectively, the number density of photons and the shape of the laser pulse. Evaluation of the first sum in (2) must be performed over states of the atomic continuum (ionization processes). Finally, n_a, n_e are, respectively, the atomic ground-state and electronic population densities.

In (2), the following assumptions are made:

Diffusion is neglected for excited states since characteristic times for this process are longer than the mean lifetime of these states. This assumption is not necessary verified for metastable states.

Three-body atomic collisions are neglected, since we are dealing with low-pressure studies; but these processes can be easily taken into account.

Collisions between two excited atoms are neglected compared to collisions between excited and ground-state atoms since $N_i(t) \ll n_a(t)$, $|i\rangle \neq |\text{ground state}\rangle$. This assumption leads to linearization of the rate equations.

Saturation effects (power broadening, dynamical Stark effect) are not taken into account in the optical pumping process[16] and no attention is paid to fine spectral resolution.

Photoionization induced by laser radiation is also neglected, compared to bound-bound absorption. This assumption can be experimentally checked.[16]

Electronic and ground-state atomic populations are not affected by laser radiation. This means that $n_e = n_e^0$, $E_e = E_e^0$ (electronic kinetic energy) and $n_a = n_a^0 = P_a/kT_g$ (P_a, T_g, respectively, pressure and gas temperature). This hypothesis holds, provided the pumping process does not start from the ground state.

When the laser is off, the ionized gas is in a quasistationary equilibrium:

$$\frac{dN_i^0}{dt} = 0. \tag{3}$$

With the laser radiation acting, one has, for example, $n+1$ levels whose populations are effectively perturbed:

$$N_i(t) = N_i^0 + \Delta N_i(t), \quad i = 1,2,\ldots,n+1. \tag{4}$$

Combining (3) and (4) in (2), we obtain the perturbed rate equations:

$$\frac{d\Delta N_i}{dt} = -\Delta N_i\left(\sum_{k<i}(A_{ik}\Lambda_{ik}) + n_a^0\sum_{k\neq i}R_{ik} + n_e^0\sum_{k\neq i}S_{ik}\right) + \sum_{j\neq i}\Delta N_j(A_{ji}\Lambda_{ji} + n_a^0R_{ji} + n_e^0S_{ji}) + \delta_{ia}N_b n_p\sigma_{ba}L(t)$$
$$-\delta_{ib}N_b n_p\sigma_{ba}L(t), \quad \Delta N_i(t_0) = \Delta N_i^0, \quad i,j = 1,2,\ldots,n+1. \tag{5}$$

Taking for initial condition in (5) a time t_0 such that $L(t > t_0) = 0$, we obtain an homogeneous system describing the laser-free relaxation of the perturbed populations. If in this regime, the collisional processes starting from $|b\rangle$ to populate the $|i\rangle$ states can be entirely neglected, one can remove from (5) an equation corresponding to the $|b\rangle$-state population. Then this state just acts as a population reservoir.

With this assumption, Eq. (5) becomes

$$\frac{d\Delta\vec{N}}{dt} = A\Delta\vec{N}, \quad \Delta\vec{N}(t_0) = \Delta\vec{N}_0$$

with

$$\Delta\vec{N} = \begin{pmatrix} \Delta N_1 \\ \Delta N_2 \\ \cdot \\ \cdot \\ \cdot \\ \Delta N_i \\ \cdot \\ \cdot \\ \cdot \\ \Delta N_n \end{pmatrix}, \quad i \neq b \tag{6}$$

and

$$\Delta N_b(t) = \sum_{\substack{i=1 \\ \neq b}}^{n} \Delta N_i(t) + \xi(t), \tag{7}$$

where A is a square matrix of order n, $\Delta\vec{N}(t)$ being the perturbed population vector at time t. Equation (7) expressed conservation of the particle number at each time when $\xi(t)$ represents population variations induced from states $|i\rangle$ on states $|k\rangle \neq |j\rangle$ [see first sum in Eq. (5)], the perturbed populations of which do not intervene explicitly in the rate equations (5) and (6).

In Eq. (6), the term a_{ij} $(i \neq j)$ represents the coefficient of the reactions leading to formation of state $|i\rangle$ from state $|j\rangle$. This term is positive and generally has the form

$$a_{ij} = \alpha_{ij} + \sum_{\phi} \beta_{ij}^{\phi}\phi . \tag{8}$$

β_{ij} is the rate of the $|j\rangle \rightarrow |i\rangle$ transfer reaction induced by a process characterized by the physical quantity ϕ (n_a, n_e, for example). α_{ij} is the coefficient of spontaneous transformation from $|j\rangle$ to $|i\rangle$ (radiation emission).

The diagonal term a_{ii} corresponds to the total quenching coefficient of state $|i\rangle$ and is therefore negative. Generally, a_{ii} is given as

$$a_{ii} = -a_{ki} - \sum_{\substack{j=1 \\ \neq i}}^{n} a_{ji} , \tag{9}$$

where a_{ki} corresponds to the loss of population from $|i\rangle$ to the outside of the system described by Eq. (6) (diffusion, associative ionization, spontaneous emission, etc.).

Then, the matrix A may be written

$$A = \alpha + \sum_{\phi} \beta^{\phi}\phi , \tag{10}$$

where $\alpha = \{\alpha_{ij}\}$ and $\beta^{\phi} = \{\beta_{ij}^{\phi}\}$ are square matrices of order n, and ϕ is determined by the experimental conditions, that is gas pressure and temperature, and current intensity.

This description of the perturbed rate equations is a special case of the general theory of transformation systems whose axiomatics is developed in Ref. 17.

Now, the problem is to identify α and β from measurements of $\Delta N_i(t)$: $\Delta N_i(t)$, $i = 1, \ldots, n$ being the solution of Eq. (6).

The relaxation matrix A is determined so as to minimize the difference between the experimental values and those calculated from the model. This method, recently developed in numerical analysis and named "identification problem," is presented in the Appendix for the special case of Eq. (6).

III. EXCITATION TRANSFER IN THE $N = 3$ HELIUM SUBLEVELS

A. Experimental setup

The experimental setup was described in previous laser perturbation studies.[12-14] Let us only recall that a tunable dye laser excited by a nitrogen laser ($P_L < 1$ kW/pulse, pulse width 4 ns, spectral width ~0.2 Å) is used to induce a selective perturbation of the $3\,^{2S+1}L$ sublevel of helium by pumping of the $2\,^{2S+1}L \pm 1 \rightarrow 3\,^{2S+1}L$ transition.

The helium plasma is produced in a capillary glow discharge (pressure range $P_{He} = 0.2$–7 Torr, current intensity $i = 10$–40 mA). For different experimental conditions, corresponding values of electronic density have been measured by microwave techniques (Fig. 1), and electronic kinetic energy calculated from glow-discharge theory ($3 < E_e < 20$ eV). Gas temperature is measured with a thermocouple in contact with the discharge tube: $T_g = 325 \pm 5$ K. The discharge is longitudinally traversed by the laser beam, and fluorescence light emitted by a cross section of the positive column is observed in a perpendicular direction by means of a 1.15-m grating spectrometer and a photomultiplier. Time dependence of the fluorescence light is analyzed by a PAR 162 boxcar averager giving a time resolution of 5 ns. The detection system is calibrated for absolute intensity measurements with a tungsten-ribbon filament lamp after determination of the background.[16] In fact, due to linearity of the rate equations (6), only relative intensity calibration is needed.

B. Experimental results and numerical identification

A partial diagram of helium $n = 2, 3$ atomic energy states is shown in Fig. 2.

The relaxations of population $\Delta N_i(t)$ for the $|i\rangle = 3\,^{2S+1}L$ states ($S = 0, 1$; $L = S, P, D$), induced by

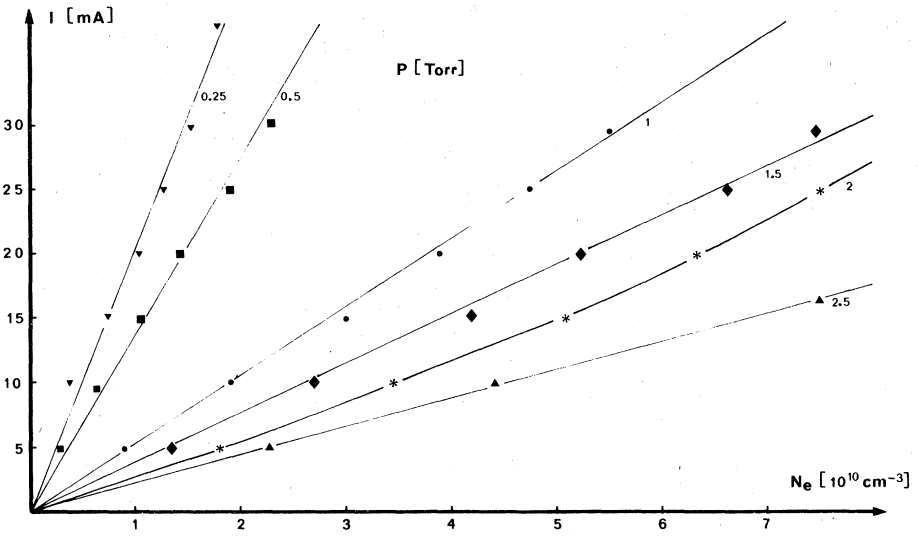

FIG. 1. Electronic density number in the discharge versus current intensity i for various values of the helium pressure.

laser optical pumping of the six transitions drawn in Fig. 2, have been successively studied for various discharge conditions (P_{He}, i), yielding six independent sets of experimental results. In fact, for the six experiments, and in the pressure range investigated, we observe the following transfers: $2\,^1S$-$3\,^1P$ pumped, $3\,^1P \rightleftharpoons 3\,^1D$ excitation transfer; $2\,^1P$-$3\,^1D$ pumped, $3\,^1P \rightleftharpoons 3\,^1D$ excitation transfer; $2\,^1P$-$3\,^1S$ pumped, no transfer; $2\,^3S$-$3\,^3P$ pumped, no transfer; $2\,^3P$-$3\,^3D$ pumped, $3\,^3D \rightleftharpoons 3\,^3P$ excitation transfer; $2\,^3P$-$3\,^3S$ pumped, no transfer.

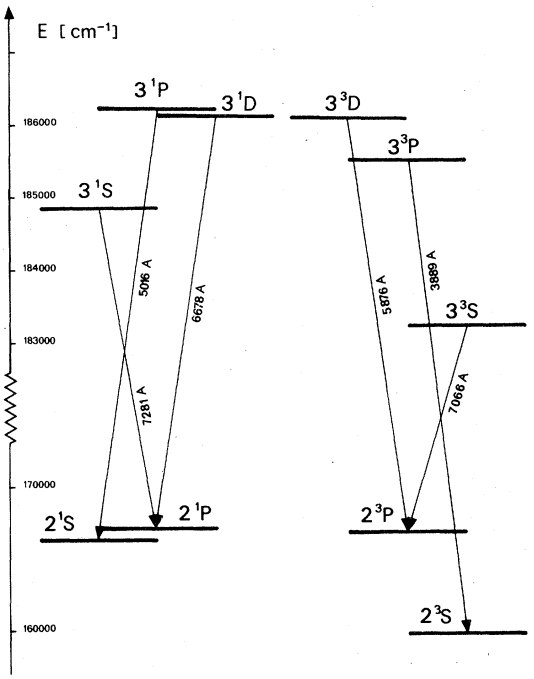

FIG. 2. Partial energy diagram of helium atomic states involved in the experiment.

Then the quenching and excitation transfer coefficients a_{ij} are determined for each experimental situation by the identification procedure (see the Appendix). As an example, the $2\,^1S$-$3\,^1P$ perturbation experiment analysis will be fully described. For the other experiments, only the essential features will be given.

1. $3\,^1P$ population perturbation

In this experiment, the $2\,^1S \rightarrow 3\,^1P$ transition was pumped ($\lambda_L = 5016$ Å; dye, C30 + 7D4MC). The laser spectral width exceeds the atomic linewidths so that the whole atomic velocity distribution is pumped.

In the pressure range investigated, induced fluorescence was only observed in the $3\,^1D$-$2\,^1P$ transition. Particularly, no transfer was detected in the triplet and in the $n=4$ systems, so that the perturbed rate equation system reduces to the $3\,^1P$ and $3\,^1D$ states:

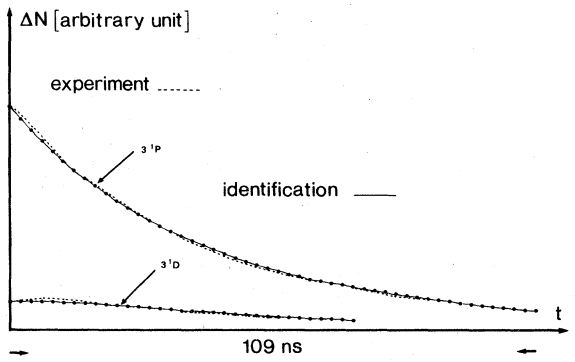

FIG. 3. Typical numerical identification of the relaxation curves in the $3\,^1P$ pumping experiment (P_{He} = 0.7 Torr, i = 20 mA, E = 2.5%).

$$\frac{d\Delta N_{3^1P}}{dt} = -\Delta N_{3^1P}\Big(A_{3^1P-1^1S}\Lambda_{3^1P-1^1S} + A_{3^1P-2^1S}\Lambda_{3^1P-2^1S} + A_{3^1P-3^1D}\Lambda_{3^1P-3^1D} + A_{3^1P-3^1S}\Lambda_{3^1P-3^1S} + n_{\mathrm{He}}\sum_k R_{3^1P-k} + n_e\sum_k S_{3^1P-k}\Big) + \Delta N_{3^1D}(n_{\mathrm{He}}R_{3^1D-3^1P} + n_e S_{3^1D-3^1P}),$$

$$\frac{d\Delta N_{3^1D}}{dt} = -\Delta N_{3^1D}\Big(A_{3^1D-2^1P}\Lambda_{3^1D-2^1P} + n_{\mathrm{He}}\sum_k R_{3^1D-k} + n_e\sum_k S_{3^1D-k}\Big) + \Delta N_{3^1P}(n_{\mathrm{He}}R_{3^1P-3^1D} + A_{3^1P-3^1D}\Lambda_{3^1P-3^1D} + n_e S_{3^1P-3^1D}), \tag{11}$$

with notations of Sec. II.

Recordings of the 5016-, 7281-, and 6678-Å line profiles show that no radiative reabsorption occurs for these transitions so that

$$\Lambda_{3^1P-2^1S} = \Lambda_{3^1D-2^1P} = \Lambda_{3^1P-3^1D} = \Lambda_{3^1P-3^1S} = 1.$$

The experimental relaxation curves $\Delta N_{3^1P}(t)$ and $\Delta N_{3^1D}(t)$ have been identified to Eq. (11) for $i = 10$ and 20 mA and for five to eight values of P_{He} in the 0.3–7-Torr range. As an example, identification of the experiment $P = 0.7$ Torr, $i = 20$ mA is shown in Fig. 3.

Coefficients a_{ij}^{id} of the identified matrix A^{id} are reported in Fig. 4 as a function of pressure $P_{\mathrm{He}} = n_{\mathrm{He}}/kT_g$ for $i = 20$ mA, and in Fig. 5 as a function of current intensity i for different values of P_{He}, with

$$\begin{aligned}
a_{11} &= -\Big(A_{3^1P-1^1S}\Lambda_{3^1P-1^1S} + A_{3^1P-2^1S} + A_{3^1P-3^1D} + A_{3^1P-3^1S} + n_{\mathrm{He}}\sum_k R_{3^1P-k} + n_e\sum_k S_{3^1P-k}\Big) \\
&= \alpha_{11} + n_{\mathrm{He}}\beta_{11}^P + n_e\beta_{11}^i, \\
a_{12} &= n_{\mathrm{He}}R_{3^1D-3^1P} + n_e S_{3^1D-3^1P} \\
&= n_{\mathrm{He}}\beta_{12}^P + n_e\beta_{12}^i, \\
a_{21} &= A_{3^1P-3^1D} + n_{\mathrm{He}}R_{3^1P-3^1D} + n_e S_{3^1P-3^1D} \\
&= \alpha_{21} + n_{\mathrm{He}}\beta_{21}^P + n_e\beta_{21}^i, \\
a_{22} &= -\Big(A_{3^1D-2^1P} + n_{\mathrm{He}}\sum_k R_{3^1D-k} + n_e\sum_k S_{3^1D-k}\Big) \\
&= \alpha_{22} + n_{\mathrm{He}}\beta_{22}^P + n_e\beta_{22}^i.
\end{aligned} \tag{12}$$

As can be seen in Fig. 5, there is no significant dependence of the a_{ij}'s on current intensity i so that one can neglect in Eqs. (11) and (12) the quenching and transfer mechanisms induced by electronic collisions. This observation agrees well with recent experimental data[3,18] and could be predicted from the low ionization rate of the discharge.

Then, a_{ij} becomes

$$a_{ij} \approx \alpha_{ij} + n_{\mathrm{He}}\beta_{ij}^P$$

and α_{ij}, β_{ij}^P are determined from the curves $a_{ij} = f(P_{\mathrm{He}})$ by linear regression. Coefficients α_{ij} are spontaneous-emission coefficients, whereas coefficients β_{ij}^P are atom-atom collisional rates. These are related to thermally averaged cross sections by the relation

$$\sigma_{ij} = |\beta_{ij}^P|/(8RT_g/\pi M)^{1/2},$$

where R is the ideal-gas constant and M is the reduced mass of the colliding partners.

The radiative coefficients and collisional cross sections averaged on the two current experiments are reported in Table I.

From these results, one can extract further information. Indeed, in this experiment, one has

$$\begin{aligned}
\beta_{11}^P &\approx R_{3^1P-3^1D} + R_{\mathrm{ion}}^{3^1P} = \beta_{21}^P + R_{\mathrm{ion}}^{3^1P}, \\
\beta_{22}^P &\approx R_{3^1D-3^1P} + R_{\mathrm{ion}}^{3^1D} = \beta_{12}^P + R_{\mathrm{ion}}^{3^1D},
\end{aligned} \tag{13}$$

where $R_{\mathrm{ion}}^{3^1P,3^1D}$ represents the rate coefficient for associative ionization[19]:

$$\mathrm{He}(3^1P, 3^1D) + \mathrm{He}(1^1S) \rightarrow \mathrm{He}_2^+ + e^- + \Delta E.$$

From (13) one thus can deduce $R_{\mathrm{ion}}^{3^1P}$ and $R_{\mathrm{ion}}^{3^1D}$ and the corresponding thermally averaged cross sections. Their values are given in Table I.

Going back to Fig. 4, one finds that for $P_{\mathrm{He}} \leq 0.5$ Torr, a_{11} deviates from the straight line obtained for higher pressure. This result is quite significant; it corresponds to escape of radiation in the 3^1P-1^1S transition ($\Lambda_{3^1P-1^1S} \neq 0$) which is, on the contrary, entirely trapped for $P_{\mathrm{He}} > 0.5$ Torr ($\Lambda_{3^1P-1^1S} = 0$). This effect was specially studied in[11] by the same experimental method.

2. 3^1D population perturbation

Pumping the 2^1P-3^1D transition ($\lambda_L = 6678$ Å; dye, R6G + CVP), this experiment leads in an independent way to the determination of the same 3^1P, 3^1D radiative coefficients and collisional rates, but from the "inverse" pumping mechanism. Results are in excellent agreement with the previous ones.[16] This represents an important check on the coherence and accuracy of the developed experimental and numerical methods.

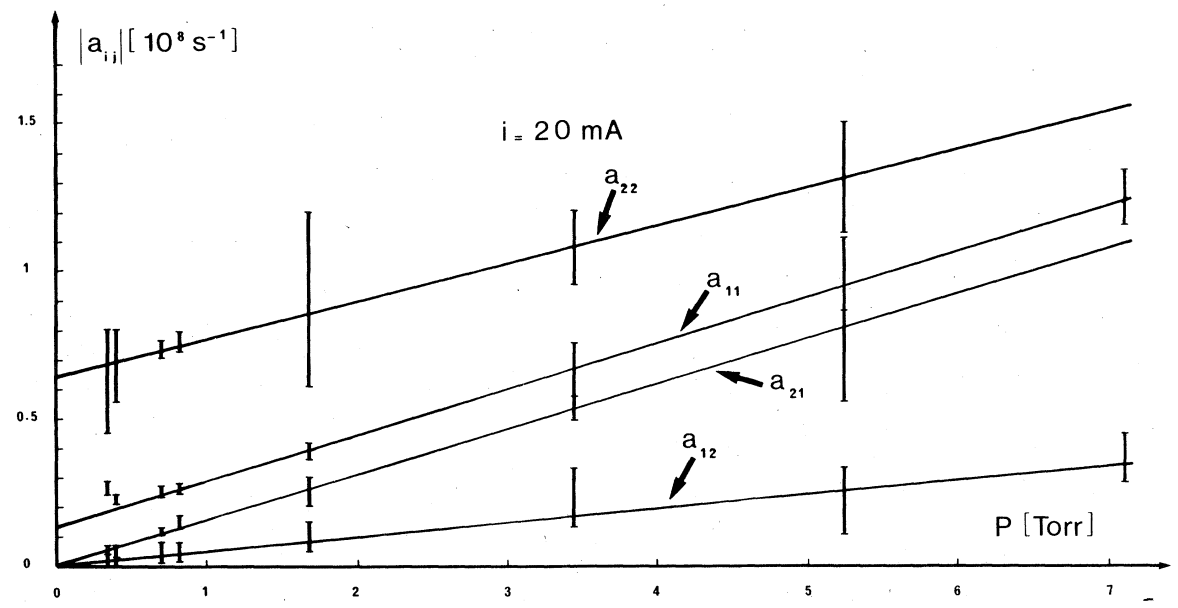

FIG. 4. Variations of the coefficients a_{ij} deduced from the $3\,^1P$ pumping experiments as a function of P_{He} for $i=20$ mA.

3. $3\,^1S$ population perturbation

In this experiment, the $2\,^1P \rightarrow 3\,^1S$ transition ($\lambda_L = 7281$ Å; dye, oxazine 725) was pumped and no transfer was observed so that monoexponential analysis of the relaxation curves is appropriate for determining the quenching coefficient

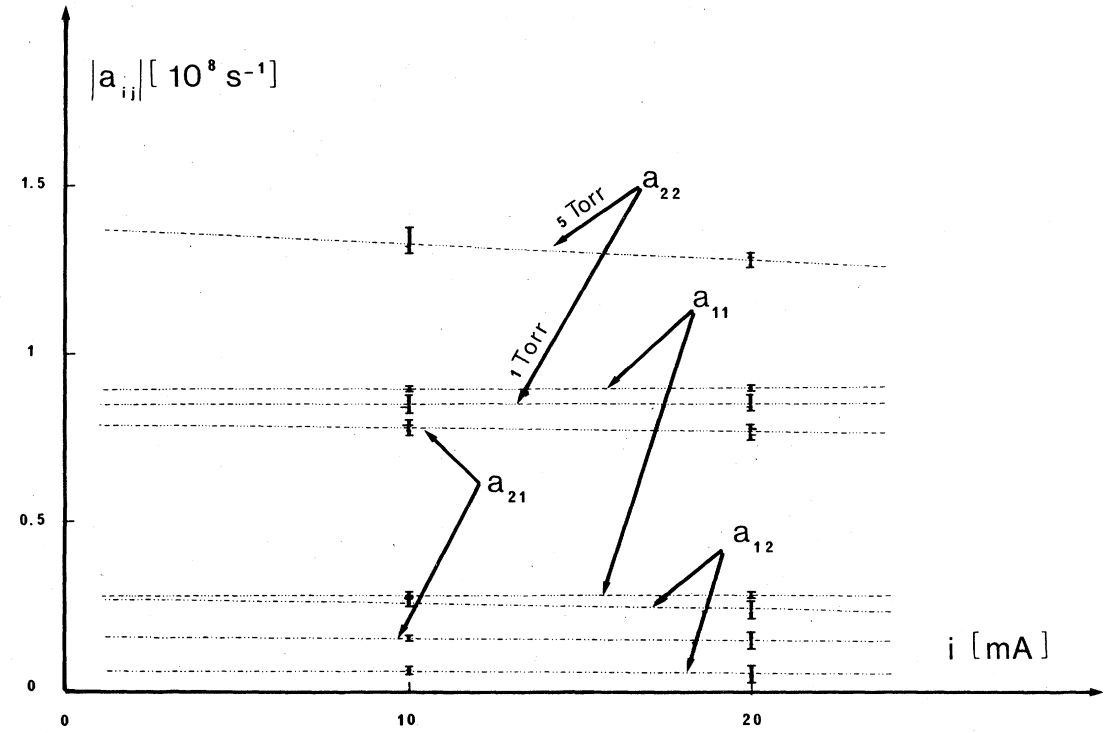

FIG. 5. Variations of the coefficients a_{ij} deduced from the $3\,^1P$ pumping experiments as a function for i for different values of P_{He}.

TABLE I. Mean radiative coefficients $\bar{\alpha}_{ij}$ and collisional quenching $\bar{\sigma}_{ii}$; excitation transfer ($\bar{\sigma}_{ij}$) and associative ionization ($\bar{\sigma}_{\text{ion}}$) cross sections for the $3\,^1P$-$3\,^1D$ system.

$\bar{\alpha}_{11} = -0.1293 \pm 0.003 \times 10^8\ s^{-1}$	$\bar{\sigma}_{11} = 28.00 \pm 0.8$ Å^2
$\bar{\alpha}_{21} = 0.000 \pm 0.003 \times 10^8\ s^{-1}$	$\bar{\sigma}_{21} = 27.8 \pm 1.2$ Å^2
$\bar{\alpha}_{12} = 0.000$	$\bar{\sigma}_{12} = 9.9 \pm 0.3$ Å^2
$\bar{\alpha}_{22} = -0.614 \pm 0.009 \times 10^8\ s^{-1}$	$\bar{\sigma}_{22} = 25.5 \pm 1.1$ Å^2
$\bar{\sigma}^{3\,^1D}_{\text{ion}} = 15.60 \pm 1.4$ Å^2	$\bar{\sigma}^{3\,^1P}_{\text{ion}} = 0.2 \pm 0.2$ Å^2

$$a_{11} = -\left(A_{3\,^1S-2\,^1P}\Lambda_{3\,^1S-2\,^1P} + n_{\text{He}}\sum_k R_{3\,^1S-k} + n_e \sum_k S_{3\,^1S-k}\right).$$

Since no variation with n_e was observed, and with $\Lambda_{3\,^1S-2\,^1P} = 1$, one has

$$\alpha_{11} = -A_{3\,^1S-2\,^1P} \quad \text{and} \quad \beta^P_{11} = -\sum_k R_{3\,^1S-k}.$$

Collisional quenching of the $3\,^1S$ state can be mainly attributed to associative ionization process since no transfer has been detected. Coefficients and cross sections are reported in Table II.

4. $3\,^3S$ population perturbation

In helium glow discharge, the $n = 3$ triplet lines show a partly resolved doublet structure, so that the laser pumping process can affect either one or two components according to their frequency separation. In fact, this causes particular analysis only for the $3\,^3D$ experiment.

Pumping the $2\,^3P_{1,2}$-$3\,^3S_1$ transition ($\lambda_L = 7065$ Å; dye, N.B.), one observes no induced fluorescence; so that as for the $3\,^1S_1$ state, a monoexponential analysis of the $3\,^3S_1$ relaxation curves gives

$$\alpha_{11} = -A_{3\,^3S_1 \to 2\,^3P_{0,1,2}}$$

and

$$\beta^P_{11} = -\sum_k R_{3\,^3S_1-k}$$

(Table II).

5. $3\,^3P$ population perturbation

In this experiment ($2\,^3S_1 \to 3\,^3P_{0,1,2}$ transition;

TABLE II. Summary of the radiative coefficients and collisional cross sections obtained by the present method and comparison with previous theoretical and experimentals values.

	State	Present experiment		Ref. 26	Ref. 27 (320 K)	Ref. 8 (300 K)		Ref. 3 (320 K)	
Radiative coefficients ($10^8\ s^{-1}$)	$3\,^1S$	0.18	±0.01	0.181					
	$3\,^1P$	0.13	±0.01	0.135					
	$3\,^1D$	0.63	±0.04	0.638					
	$3\,^3S$	0.279	±0.008	0.278		0.29	±0.03		
	$3\,^3P$	0.0986	±0.003	0.105		0.091	±0.02		
	$3\,^3D$	0.656	±0.007	0.666		0.6	±0.15		
Excitation transfer cross sections (Å^2)	$3\,^1D \rightleftarrows 3\,^1S$		<0.1						<0.04
	$3\,^1P \to 3\,^1D$	27	±2					32	±1
	$3\,^1D \to 3\,^1P$	10	±2					10.6	±0.7
	$3\,^3D \rightleftarrows 3\,^3S$		<0.1		6×10^{-6}				<0.01
	$3\,^3P \to 3\,^3D$	0.15	±0.10		0.26	0.098	±0.02	0.067	±0.005
	$3\,^3D \to 3\,^3P$	1.2	±0.2		1.02			0.62	±0.05
	$3\,^1P \to 3\,^1S$		<0.1					4.5	±0.03
	$3\,^3P \to 3\,^3S$		<1		1.8	2.62	±0.24	2.9	±0.3
Associative ionization cross sections (Å^2)	$3\,^1S$		<3.7						<0.1
	$3\,^1P$	1	±1					3.1	±1
	$3\,^1D$	15	±4					20	±4
	$3\,^3S$		<0.3		0.07				<0.01
	$3\,^3P$		<4		1.9			1.6	±0.1
	$3\,^3D$	2.4	±0.5		2.8			4.5	±0.5
Collisional quenching cross sections (Å^2)	$3\,^1S$	3.7	±0.4						<0.1
	$3\,^1P$	28	±2					36	±2
	$3\,^1D$	25	±2					31	±5
	$3\,^3S$	0.3	±0.3		0.07	0.15	±0.05		<0.01
	$3\,^3P$	5.5	±0.3		4	4	±0.3	4.6	±0.4
	$3\,^3D$	3.6	±0.3		3.8	3.9	±0.3	5.1	±0.6

$\lambda_L = 3888.65$ Å; dye, B.B.Q.) no induced fluorescence was detected. An analysis of the monoexponential $3\,^3P$ relaxation curves determines

$$\alpha_{11} = -\left(A_{3\,^3P_{0,1,2}\rightarrow 2\,^3S_1} + A_{3\,^3P_{0,1,2}\rightarrow 3\,^3S_1}\right)$$

and

$$\beta_{11}^P = -\sum_k R_{3\,^3P-k}$$

(Table II).

6. $3\,^3D$ population perturbation

In this experiment, the $2\,^3P_{2,1}\rightarrow 3\,^3D_{1,2,3}$ transition was pumped ($\lambda_L = 5875.62$ Å; dye, R6G), and the corresponding resonance fluorescence was only detected in this transition. The $2\,^3P_0\rightarrow 3\,^3D_1$ component ($\lambda = 5875.97$ Å) of the triplet was not pumped or detected.

Induced fluorescence in the $3\,^3P_{0,1,2}\rightarrow 2\,^3S_1$ transition is effective for $P_{He} \geq 4$ Torr. In this pressure range, the identification method gives as in Sec. III B 1 the following coefficients:

a_{11}:

$$\begin{cases} \alpha_{11} = -\left(A_{3\,^3D_{3,2,1}\rightarrow 2\,^3P_{2,1}} + A_{3\,^3D_{3,2,1}\rightarrow 3\,^3P_{0,1,2}}\right), \\ \beta_{11}^P = -\sum_k R_{3\,^3D-k}\ ; \end{cases}$$

a_{12}:

$$\begin{cases} \alpha_{12} = 0\ , \\ \beta_{12}^P = R_{3\,^3P\rightarrow 3\,^3D}\ ; \end{cases}$$

a_{21}:

$$\begin{cases} \alpha_{21} = A_{3\,^3D_{1,2,3}\rightarrow 3\,^3P_{0,1,2}}\ , \\ \beta_{21}^P = R_{3\,^3D\rightarrow 3\,^3P}\ ; \end{cases}$$

a_{22}:

$$\begin{cases} \alpha_{22} = -\left(A_{3\,^3P_{0,1,2}\rightarrow 2\,^3S_1} + A_{3\,^3P_{0,1,2}\rightarrow 3\,^3S_1}\right), \\ \beta_{22}^P = -\sum_k R_{3\,^3P-k}\ . \end{cases}$$

Coefficients α_{22} and β_{22}^P are identical, respectively, to coefficients α_{11} and β_{11}^P of the $3\,^3P$ experiment. Excellent agreement is found between these two independent experiments. In Table II the mean values of these coefficients are given together with other coefficients and cross sections.

For $P_{He} < 1.5$ Torr, the monoexponential analysis of the $3\,^3D$ population yields a_{11} coefficients which are greater than those deduced from the extrapolated straight line (Fig. 6). This systematic behavior (different experiments led to the same results) indicates that an additional quenching mechanism for the studied states must be taken

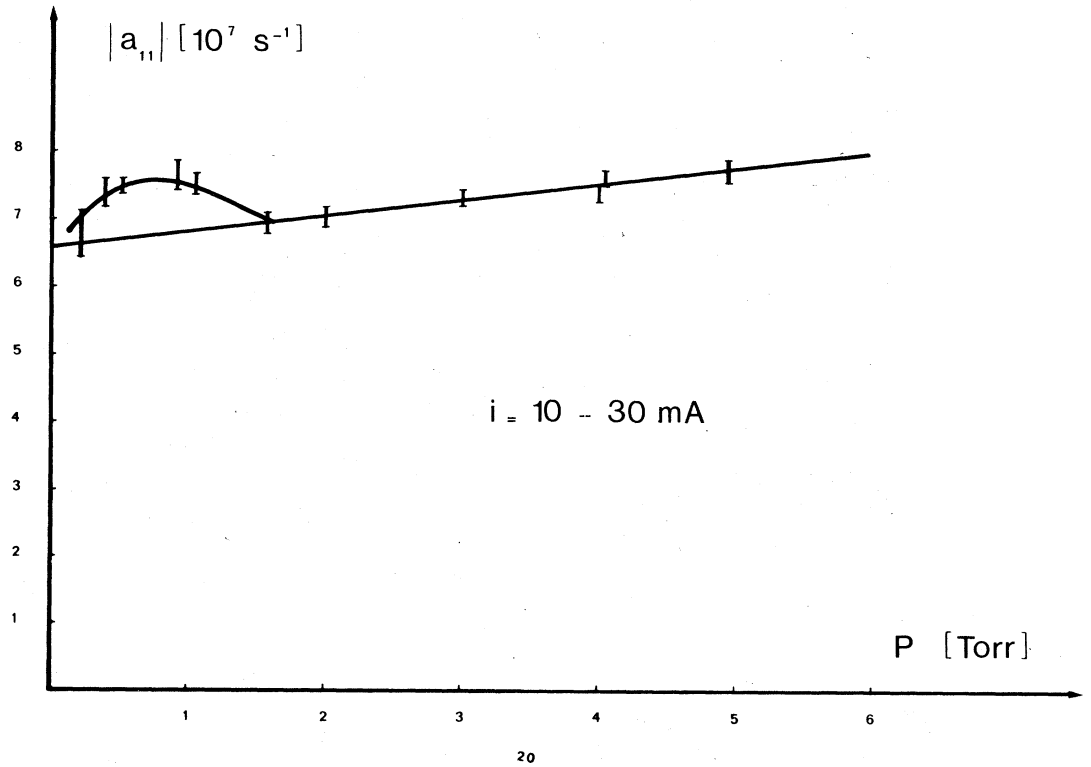

FIG. 6. Variations of the quenching coefficient of the $3\,^3D$ level with gas pressure.

into account in this pressure range.

One can explain this effect as being due to collisional excitation transfer from $3\,^3D_{3,2}$ states towards $3\,^3D_1$ states which is not entirely equilibrated by the reverse process in the low-pressure regime despite the low energy gap involved. This assumption has been checked first from measurements of the intensity ratio of the two components as a function of pressure, and, in a recent experiment in which pumping the $2\,^3P_0 \rightarrow 3\,^3D_1$ transition was involved; we observe collisional transfer on the $3\,^3D_{3,2}$ sublevels[20] with a thermally averaged cross section in the 200-Å^2 range.

These results are indicative of the spin-orbit-coupling effect in near-resonant atom-atom collisions at thermal energy.

IV. CONCLUSION

Radiative coefficients and collisional cross sections determined by the laser-perturbation method are arranged and compared with other work in Table II.

Radiative coefficients

$$A_i = \sum_{k<i} A_{i-k}$$

are in excellent agreement with the tabulated values given by Wiese *et al.*[21]

Collisional cross sections for the triplet system are on the whole in agreement with experimental values of Gauthier *et al.*,[8] who used a similar laser-perturbation technique to study excitation transfer in the $n=3$ triplet system of a helium afterglow from $2\,^3S \rightarrow 3\,^3P$ transition pumping, and with theoretical calculations of Cohen,[22] who developed an *ab initio* model of the He_2 diabatic states.

Excitation transfers in a helium glow discharge were studied by Wellenstein and Robertson.[3] In this experiment the $n=3$ sublevel populations were perturbed by absorption of radiation originating from a helium lamp. Assuming quenching coefficients a_{ii} known from early measurements, they deduced excitation transfer rates from comparison of the time-independent population rate equations ($d\Delta N_i/dt = 0$) with the measured enhanced populations ΔN_i. Indeed, for given discharge conditions (P, i), measurements of the $n=3$ stationary perturbed populations ΔN_i are not sufficient to determine the n^2 coefficients of matrix A. But, knowledge of the a_{ii}'s reduces the unknowns to $n^2 - n$, that is to six in the present case.

Comparison with our results shows some differences both for the singlet and triplet system but specially for $3\,^1P$ and $3\,^1D$ quenching cross sections.

TABLE III. Experimental and theoretical excitation transfer cross-section ratios.

	This work	Microreversibility
$\bar{\sigma}_{3\,^1P-3\,^1D}/\bar{\sigma}_{3\,^1D-3\,^1P}$	2.7 ± 0.9	2.74
$\bar{\sigma}_{3\,^3P-3\,^3D}/\bar{\sigma}_{3\,^3D-3\,^3P}$	0.13 ± 0.10	0.127

As a supplementary check on our experimental cross sections, we have compared the ratios $\sigma_{3\,^1P-3\,^1D}/\sigma_{3\,^1D-3\,^1P}$ and $\sigma_{3\,^3P-3\,^3D}/\sigma_{3\,^3D-3\,^3P}$, respectively, to theoretical values given by the microreversibility principle. Agreement is rather good, as reported in Table III.

As a general result of our measurements, collisional excitation transfers in the $n=3$ triplet helium system are largely weaker than in the singlet system. For $P_{He} < 5$ Torr, the triplet sublevels are rather uncoupled and behave independently. This leads to a nonequilibrium population distribution among them, determined by electronic excitation mechanisms and spontaneous transitions. This effect appears on intensity of the lines emitted by the discharge.

The singlet states behave differently. Except for the low-lying $3\,^1S$ state (energy gap with respect to $3\,^1P$, $3\,^1D$ states greater than 10^3 cm^{-1}), one observes excitation transfers between $3\,^1P$ and $3\,^1D$ states for pressure in the Torr range. In the 95.8-μm helium laser this transfer tends to equilibrate the $3\,^1P$ and $3\,^1D$ population densities and then reduces amplification.[1] This results from the near-resonant character of the He-He* collisional processes: $\Delta E_{3\,^1P-3\,^1D} \approx kT_g/2.5$, whereas $\Delta E_{3\,^3D-3\,^3P} \approx 2kT_g$.[23]

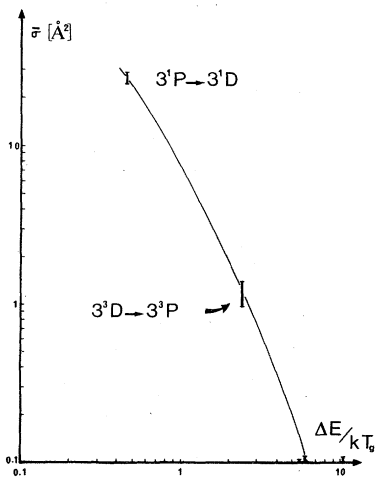

FIG. 7. Thermally averaged cross sections for excitation transfer in the $n=3$ sublevels of helium as a function of the reduced energy gap.

This quasiresonant effect appears in Fig. 7 where measured collisional cross sections are reported as a function of the reduced energy gap $\Delta E/kT_g$.

Recent investigations of collisonal excitation transfers in the $n=4$ helium structure by the same experimental method[10,24] confirm this fact. In the pressure range investigated $0.2<P_{\mathrm{He}}<3$ Torr, pumping of one transition leads to excitation transfer within all the singlet and triplet structures, so that a perturbation experiment leads in this case to eight fluorescence signals. The numerical identification procedure is being applied to the experiments. At this time, about 30 rate coefficients have been obtained with the only assumption that singlet-triplet transfers are forbidden except for F states.

ACKNOWLEDGMENTS

The authors wish to thank Dr. J. Boujot for important discussions and participation during elaboration of the numerical identification method. Calculations have been performed on the computer of the "Centre Interrégional de Calcul de la Région Centre" (Université d' Orléans).

APPENDIX: DATA ANALYSIS AND IDENTIFICATION METHOD

A. Numerical identification (Ref. 16)

Determination of α and β^{ϕ} from experiments is done in two steps. First we used linear-algebra methods by substituting in equation (6) the derivatives $d\Delta N_i(t)/dt$ by their approximate values calculated from experimental $\Delta^{\mathrm{exp}}N_i(t)$ curves at different times t_l $(l=1,\ldots,m)$ of the relaxation.

When m exceeds the system order n, we obtain an overdetermined linear system which can be resolved by a least-squares method.[16] The problem is equivalent to minimizing the functions

$$K_i(A)=\sum_{l=1}^{m}\left[\left(\frac{d\Delta N_i(t)}{dt}\right)_{t=t_l}^{\mathrm{exp}}-\sum_{j=1}^{n}a_{ij}\Delta N_j^{\mathrm{exp}}(t_l)\right]^2, \tag{A1}$$

$i=1,\ldots,n$, with respect to the coefficients a_{ij}, $j=1,\ldots,n$; that is to identify a linear combination of functions to their derivatives.

Results obtained by this procedure allow us to determine within 50% the largest coefficients of A, whereas the other ones are undetermined. The lack of accuracy of this numerical approach is a consequence of derivative calculations on noisy experimental curves.

In fact, this method is used only as a first approximation of a more refined solution, provided that the undetermined coefficients a_{ij} verify the conditions $a_{ij}>0$, $i\neq j$, and $a_{ii}<0$. Later on, we worked out an accurate identification model of the matrix A from experimental curves $\Delta N_i^{\mathrm{exp}}(t)$. This numerical method primarily developed in Refs. 25 and 26 is based on recent results obtained in the frame of transformation-system theory.[27] The principle is the following: coefficients in the matrix A are determined so as to minimize the difference between the experimental curves $\Delta N_i^{\mathrm{exp}}(t)$ and those calculated from the model [Eq. (6)].

The identification problem is then equivalent to that of finding the minimum of the error function:

$$J(A)=\sum_{i=1}^{n}\int_{t_0}^{t_1}[\Delta N_i^{\mathrm{calc}}(t,A)-\Delta N_i^{\mathrm{exp}}(t)]^2dt,$$

where $\Delta N_i^{\mathrm{calc}}(t)$ are the values corresponding to $\Delta N_i^{\mathrm{exp}}(t)$ calculated from Eq. (6) with the matrix A.

The functional framework is worked out in Ref. 27, so that we confine ourselves to description of the numerical algorithm.

We first define $\vec{\mathrm{P}}(t)$ solution of the adjoint problem:

$$-\frac{d\vec{\mathrm{P}}}{dt}=A^*\vec{\mathrm{P}}(t)-2[\Delta\vec{\mathrm{N}}_{\mathrm{calc}}(t,A)-\Delta\vec{\mathrm{N}}_{\mathrm{exp}}(t)],$$
$$\vec{\mathrm{P}}(t_1,\Delta\vec{\mathrm{N}})=0,\quad \vec{\mathrm{P}}\in R^n. \tag{A2}$$

These equations are obtained from the Lagrangian

$$\mathcal{L}(\Delta\vec{\mathrm{N}},A,\vec{\mathrm{P}})=\int_{t_0}^{t_1}\left[(\Delta\vec{\mathrm{N}}_{\mathrm{calc}}-\Delta\vec{\mathrm{N}}_{\mathrm{exp}})^2-\left(A\Delta\vec{\mathrm{N}}_{\mathrm{calc}}-\frac{d\Delta\vec{\mathrm{N}}_{\mathrm{calc}}}{dt},\vec{\mathrm{P}}\right)\right]dt$$

whose functional derivatives with respect to $\Delta\vec{\mathrm{N}}_{\mathrm{calc}}$ are zero.

With $\vec{\mathrm{P}}$ solution of Eq. (A2), the functional derivatives of the error function are given by

$$\frac{\partial J(A)}{\partial a_{ij}}=\int_{t_0}^{t_1}P_i(t)\Delta N_j^{\mathrm{calc}}(t)dt.$$

The minimum of $J(A)$ then can be obtained from the iterative-gradient algorithm[28]:

$$(a_{ij})^{(q+1)}=(a_{ij})^{(q)}-c^{(q+1)}\frac{\partial J(A)}{\partial a_{ij}},\quad i,j=1,\ldots,n$$

where q is the iteration number and c^q is a convergence coefficient.[28] Since $J(A)$ is strictly convex, the identification method has a unique solution.

The iterative process is stopped when

$$E=J(A^{q+1})\Big/\int_{t_0}^{t_1}|\Delta\vec{\mathrm{N}}|^2dt<\epsilon,$$

where ϵ is a given relative error.

The structure of numerical calculations is described in Ref. 16 and is depicted in the flow chart

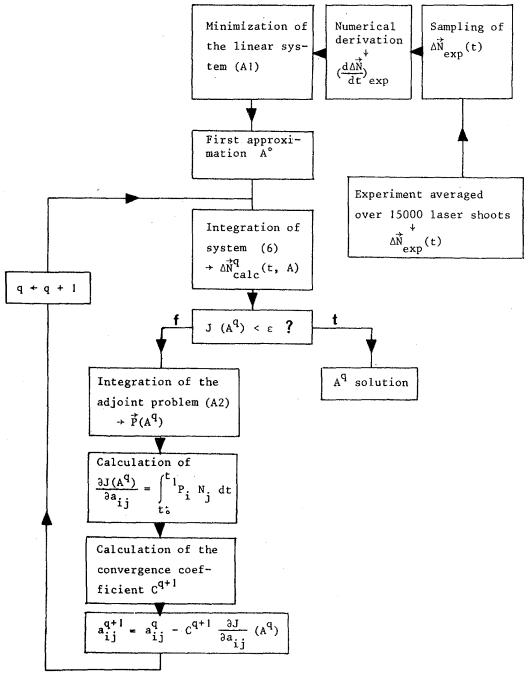

FIG. 8. Flow chart of the numerical identification procedure.

of Fig. 8. The corresponding computer program is written in FORTRAN G/SIRIS 7.

B. General results

Application of the identification program to the $n=3$ helium experiments is done with $E<3\%$. Generally the iteration number q is raised to 1500 in order to get the minimum value of $J(A)$.

In these calculations, total error $\Delta a_{ij}^{\mathrm{id}}$ on a_{ij}^{id} including numerical and experimental errors is estimated by varying the experimental values $\Delta N_i^{\mathrm{exp}}(t_l)$ within their error bars. The scattering obtained on the a_{ij} values then is representative of experimental errors combined with inherent errors. These ones can be evaluated theoretically[29] and numerically.[16]

Simulations of an ideal experiment indicate that inherent errors are less than 10^{-4} and are negligibly small compared to errors on $\Delta N_i^{\mathrm{exp}}(t)$, estimated to be 5%. Correlations between experimental errors and total identification errors $\Delta a_{ij}^{\mathrm{id}}$ are studied from numerical simulation of noisy curves $\Delta N_i^{\mathrm{sim}}(t_l)$. Taking a pseudorandom distribution of the data within ± 5% of the true values, we obtained in each numerical experiment $E<2\%$. Twenty such simulations were effected leading to scattering on each a_{ij} value generally less than 10%. Furthermore, in all cases the mean arithmetic values are closed within 1% to the true values.

These numerical studies allow us in practical situations to determine a realistic estimate of $\Delta a_{ij}^{\mathrm{id}}$. They provide also a check on the efficiency and accuracy of the identification method.

C. Identification of the matrices α and β

Identification of matrix A corresponds to a well-defined experiment in which ϕ is constant. Determination of α and β from A entails the knowledge of sets of experimental data obtained for different values of ϕ. A given experiment leads to the identified matrix $A^{\mathrm{id}}(\phi)$, where coefficients $a_{ij}^{\mathrm{id}}(\phi)$ are linearly dependent on ϕ through Eq. (8). $\alpha_{ij}^{\mathrm{id}}$ and β_{ij}^{id} are then determined from least-squares linear regression of $a_{ij}^{\mathrm{id}}(\phi)$ on ϕ taking into account the "confidence interval" $\Delta a_{ij}^{\mathrm{id}}(\phi)$.

D. Nonexponential analysis

When in the perturbed rate equations (6), one has $\Delta N_i(t) \gg \Delta N_j(t), j \neq i$ the terms $a_{ji}\Delta N_j(t)$ intervening in the $\Delta N_i(t)$ rate equation can be neglected compared to $a_{ii}\Delta N_i(t)$.

Then $\Delta N_i(t)$ is written

$$\Delta N_i(t) = \Delta N_i^0 e^{a_{ii}t} .$$

The time dependence of $\Delta N_i(t)$ follows an exponential law, and a_{ii} is easily determined from the plot of $\log[\Delta N_i(t)]$.

This analysis holds provided that at time $t > t_0$ populating back processes are completely negligible with respect to quenching processes:

$$|a_{ii}\Delta N_i(t)| \gg \sum_{j \neq i} |a_{ji}\Delta N_j(t)| .$$

---

*Based on part of a thesis submitted to the University of Orléans, 11 January 1979.

[1]J. S. Levine and A. Javan, Appl. Phys. Lett. 14, 348 (1969).

[2]J. Stevefelt and F. Robben, Phys. Rev. A 5, 1502 (1972).

[3]H. F. Welenstein and W. W. Robertson, J. Chem. Phys. 56, 1072 (1972); 56, 1077 (1972); 56, 1414 (1972).

[4]P. H. Wine and R. E. Glick, J. Quant. Spectrosc. Radiat. Transfer 16, 879 (1976).

[5]J. D. Jobe and R. M. St. John, Phys. Rev. A 5, 295 (1972).

[6]C. F. Burrel and H. J. Kunze, Phys. Rev. Lett. 28, 1 (1972).

[7]C. B. Collins, B. W. Johnson, and M. J. Shaw, J. Chem. Phys. 57, 5310; 57, 5317 (1972).

[8]J. C. Gauthier, J. P. Geindre, J. P. Moy, and J. F. Delpech, Phys. Rev. A 13, 1781 (1976).
[9]M. J. Shaw and M. J. Webster, J. Phys. B 9, 2839 (1976).
[10]A. Catherinot and B. Dubreuil, Orleans Report No. 76/01, 1976 (unpublished).
[11]B. Dubreuil and A. Catherinot, Physica C 93, 408 (1978).
[12]B. Dubreuil and A. Catherinot, J. Phys. D. 11, 1043 (1978).
[13]A. Catherinot, P. Placidet, and B. Dubreuil, J. Phys. B 11, 3775 (1978).
[14]A. Catherinot and B. Dubreuil, Phys. Rev. A 18, 1097 (1978).
[15]B. Dubreuil and A. Catherinot, J. Phys. (Paris) 39, 1071 (1978).
[16]B. Dubreuil, thesis, Orleans, 1979 (unpublished).
[17]P. Delattre, thesis, Toulouse, 1972 (unpublished).
[18]C. Burrel and H. J. Kunze, Phys. Rev. A 18, 2081 (1978).
[19]M. P. Teter, F. E. Niles, and W. W. Robertson, J. Chem. Phys. 44, 3018 (1966).
[20]A. Catherinot, B. Dubreuil, and G. Gousset, Phys. Rev. A (to be published).
[21]W. L. Wiese *et al.*, Natl. Stand. Ref. Data Ser. 1 (1966).
[22]J. S. Cohen, Phys. Rev. A 13, 99 (1976).
[23]N. F. Mott and H. S. W. Massey, *The Theory of Atomic Collisions* (Oxford University, New York, 1971).
[24]A. Catherinot and B. Dubreuil (unpublished).
[25]J. Lions, *Contrôle Optimal des Systèmes Gouvernês par des Équations aux Dêrivêes Partielles* (Dunod, Paris 1968).
[26]G. Chavent, in Third Symposium of the IFAC, 1973 (unpublished).
[27]J. Delforge, Appl. Math. Comp. 2, 311 (1976).
[28]J. Cea, *Optimisation: Thêorie et Algorithmes* (Dunod, Paris 1971).
[29]J. Delforge, thesis, Université Paris-Sud, 1975 (unpublished).